Supporting Information

Elucidating the essential role of hydrogen bonding and direct H-transfer in transfer hydrogenation on transition metal catalysts

Aojie Li and Srinivas Rangarajan*
Department of Chemical and Biomolecular Engineering, Lehigh University, Bethlehem, PA, 18015
*Corresponding author srr516@lehigh.edu

S1 Gas phase enthalpy corrections to NIST-derived values

DFT-GGA calculations frequently yield inaccurate thermochemical data for gas-phase molecules with C-O unsaturation. Prior to correction, the absolute error in our DFT-derived temperature-adjusted enthalpy values for reference reactions compared to NIST-derived data could reach up to 50 kJ/mol. To address this issue, we correct the enthalpies of CO, HCOOH, and HCHO by -38.6 kJ/mol, +10.81 kJ/mol, and -8.33 kJ/mol, respectively, to align with NIST-derived values for reference reaction heats. This corrections enables us to limit absolute errors in all examined gas-phase reactions to within 5 kJ/mol of NIST-derived values (Table S1).

Table S1 Enthalpy corrections for reference gas phase reactions at T = 298 K. CO(g) is stabilized by 38.6 kJ/mol, HCOOH(g) is destabilized by 10.81 kJ/mol, HCHO(g) is stabilized by

8.33 kJ/mol. The corrected DFT ΔH are in reasonable agreement with NIST values[1]. The affected reaction enthalpies are highlighted in bold.

Reference Reaction	DFT ΔH before correction (at 298.15K) (kJ/mol)	NIST ΔH (kJ/mol)	DFT ΔH after correction (at 298.15K) (kJ/mol)
$CO + H_2O \leftrightarrow$□ $CO_2 + H_2$	**-83.73**	-41.16	**-45.13**
$HCOOH \leftrightarrow$□ $CO_2 + H_2$	**-7.84**	-14.92	**-18.65**
$HCOOH \leftrightarrow$□ $CO + H_2O$	**75.89**	26.24	**26.48**
$CH_3OH + H_2O \leftrightarrow$□ $CO_2 + 3H_2$	53.82	53.31	53.82
$HCHO + H_2 \leftrightarrow$□ CH_3OH	**-99.10**	-89.1	**-90.77**
$CO + 2H_2 \leftrightarrow$□ CH_3OH	**-137.55**	-94.47	**-98.95**
$HCHO \leftrightarrow$□ $CO + H_2$	**38.45**	5.37	**8.18**
$HCHO + H_2O \leftrightarrow$□ $CO_2 + 2H_2$	**-45.28**	-35.79	**-36.95**

S2 Elementary steps for direct hydrogen transfer mechanism

For each elementary step in direct hydrogen transfer mechanism, we implemented a series of consecutive specific reactions to simulate the process of direct hydrogen transfer (Table S2), each reaction was performed by NEB calculation to finds its transition state energy. To accurately capture the hydrogen bonded structure between intermediates, we introduced new species such as "HCOOHHCHO", "$CH_3OHHCOO$" into our model, such species stand for the hydrogen-bonded structure of two reaction intermediates. For example, "$CH_3OHHCOO$" stands for a hydrogen bonded structure of CH_3OH* and HCOO*. In elementary step HCOOH* + HCOO* $\leftrightarrow$□ HCOOH* + CO_2* + H*, "HCOOHbHCOO" stands for the hydrogen bonded structure of HCOOH* with bidentate HCOO*. Similarly, "HCOOHmHCOO" is hydrogen bonded structure of HCOOH* with monodentate HCOO*.

For some elementary steps in direct hydrogen transfer route, some specific reactions like the rotation of HCOO molecule from bidentate to monodentate configuration, would not have significant activation barrier and have trivial contribution to the overall elementary step. Therefore, we would congregate these specific reactions to the reaction before or after them.

Table S2 Direct Hydrogen Transfer route elementary steps and its specific reactions that were implemented in MKM.

Direct Hydrogen Transfer reactions	**Specific reactions implemented in MKM**
R14 COOH* + OH* ↔□ CO_2* + H_2O*	R14(a) COOH* + OH* ↔□ COOHOH*
	R14(b) COOHOH* ↔□ CO_2* + H_2O*
R22 HCHO* + HCOOH* ↔□ CH_2OH* + HCOO*	R22(a) HCHO* + HCOOH* ↔□ HCOOHHCHO*
	R22(b) HCOOHHCHO* ↔□ $HCOOCH_2OH$*
	R22(c) $HCOOCH_2OH$* + * ↔□ CO_2CH_2OH* + H*
	R22(d) CO_2CH_2OH* ↔□ CO_2(g) + CH_2OH* + *
R23 HCHO* + COOH* ↔□ CH_2OH* + CO_2*	R23(a) HCHOCOOH* ↔□ CH_2OHCOO*
	R23(b) CH_2OHCOO* ↔□ CO_2(g) + CH_2OH* + *
R24 CH_3O* + COOH* ↔□ CH_3OH* + CO_2*	R24(a) CH_3O* + COOH* ↔□ CH_3OHCOO*
	R24(b) CH_3OHCOO* ↔□ CH_3OH* + CO_2(g) + *
R25 CH_3O* + HCOOH* ↔□ CH_3OH* + HCOO*	R25(a) CH_3O* + HCOOH* ↔□ $CH_3OHHCOO$*
	R25(b) $CH_3OHHCOO$* + * ↔□ HCOO* + CH_3OH(g) + *
R26 HCOOH* + HCOO* ↔□ HCOOH* + CO_2* + H*	R26(a) HCOOH* + HCOO* ↔□ HCOOHbHCOO*
	R26(b) HCOOHbHCOO* ↔□ HCOOHmHCOO* + *
	R26(c) HCOOHmHCOO* + HCOO* ↔□ HCOOHbHCOO* + CO_2(g) + H*

S3 DFT structure of the most stable adsorption states of intermediates on Cu(111).

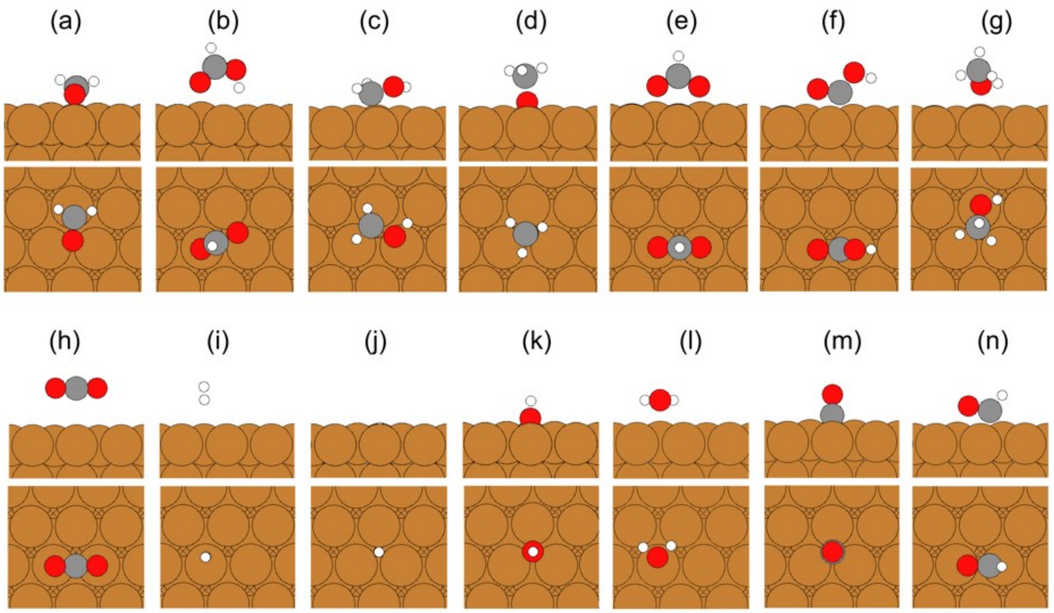

Figure S1: Most stable adsorption states of intermediates in our reaction network on Cu(111). For each row, the top part is the front view, and the bottom part is the top view. First row: (a) formaldehyde, (b) formic acid, (c) hydroxymethyl, (d) methoxy, (e) formate, (f) carboxyl, (g) methanol. Second row: (h) carbon dioxide, (i) molecular hydrogen, (j) atomic hydrogen, (k) hydroxide, (l) water, (m) carbon monoxide, (n) hydroxymethylidyne. Copper atoms are in orange, carbon in grey, oxygen in red, and hydrogen in white.

S4 Exponential factor and Shomate parameters for building the microkinetic modeling on Cu (111).

The reaction rate for adsorption/desorption steps are calculated using collision theory. The pre-exponential factor (A) that feed into MKM are showed in Table S3.

$$r^{collision} = \frac{s(T,\theta)P\theta^*}{\sqrt{2\pi m k_B T}} exp(-\frac{E_a}{k_B T})$$

To compute kinetic and thermodynamic quantities at non-zero temperatures for microkinetic modeling, entropy and enthalpy are the necessary information. Entropy is contributed by three types of degree of freedom (DOF): rotational, translational, and vibrational. While the entropy of gas phase species is determined by both of three DOFs, we assume the entropy of adsorbed species is primarily captured by the vibrational DOF, which is calculated from the frequency values, and translational and rotational modes are treated as frustrated vibrational modes. More specifically, harmonic vibrational frequencies were evaluated using VASP's implementation of the finite differences approach by computing the eigenvalue of the Hessian Matrix with respect to the position of the ions. The width of the displacement of each ion is set as 0.015Å.

$$S_{total} = S_{rot} + S_{trans} + S_{vib}$$

$$S_{vib} = R \sum_{l}^{\#ofmodes} \left(\frac{\xi_l}{e^{\xi_l}} - ln(1 - e^{-\xi_l})\right), where\ \xi_l = \frac{\hbar\omega_l}{k_B T}$$

$$H_i(T) = E_i + \sum_{l}^{\#ofmodes} \frac{1}{2}\hbar\omega_l + \int_0^T C_{p,i}(T)dT$$

The temperature-corrected entropy at different temperatures was subsequently utilized to fit a polynomial expression, which is Shomate equation. The entropy and enthalpy of all reaction intermediates and transition state energies in our microkinetic modeling was described using the Shomate equation according to NIST, and the coefficients of this polynomial expression are Shomate parameters, which constitute the parameters integrated into the MKM. Shomate parameters of intermediates and transition states are demonstrated in Table S4 and Table S5. The temperature-dependent specific heat capacity C_p, hence, could be calculated from the Shomate parameters. With all the information ensembled, we could get temperature-corrected enthalpy and zero-point energy (ZPE) corrections for our microkinetic model.

$$C_p^0 = A + B * t + C * t^2 + D * t^3 + E/t^2$$

$$H^0 - H^0_{298.15} = A * t + B * t^2/2 + C * t^3/3 + D*t^4/4 - E/t + F - H$$

$$S^0 = A * \ln(t) + B * t + C * t^2/2 + D * t^3/3 - E/(2 * t^2) + G$$

C_p = heat capacity (J/mol*K)

H^0 = standard enthalpy (kJ/mol)

S^0 = standard entropy (J/mol*K)

t = temperature (K) / 1000.

Table S3 Pre-exponential factor for adsorption/desorption steps.

Adsorption/desorption reactions	**A**
R15 HCOOH(g) + * ↔ HCOOH*	3931463461
R16 HCHO(g) + * ↔ HCHO*	4867481838
R17 CO_2* ↔ CO_2(g) + *	4020496773
R18 CH_3OH* ↔ CH_3OH(g) + *	4711878420
R19 H_2* ↔ H_2(g) + *	18785406493
R20 CO* ↔ CO(g) + *	5039594642
R21 H_2O* ↔ H_2O(g) + *	6283945748

Table S4 Shomate parameters for gaseous species and surface intermediates on clean Cu(111).

Species	**A**	**B**	**C**	**D**	**E**	**F**	**G**	**H**
CH_3OH(g)	-5.29983	181.15146	-112.57259	29.30009	0.53265	-2777.14479	185.52218	-2773.39651
CO(g)	26.41964	2.36868	9.18917	-4.99716	0.12649	-1449.37211	229.11659	-1441.74276
CO_2(g)	26.73128	51.97803	-31.76245	7.48792	-0.16811	-2185.59744	231.67315	-2175.01922
H_2(g)	30.31599	-3.69451	3.12604	0.01987	-0.03736	-627.55982	168.03767	-618.53237
H_2O(g)	28.95779	10.71881	1.75595	-0.70844	0.10546	-1315.79121	221.34129	-1307.02064
HCHO(g)	5.14178	94.58192	-47.20776	8.88903	0.55499	-2069.75315	201.97497	-2066.27721
HCOOH(g)	7.49790	154.21035	-108.96994	30.64834	0.03472	-2784.41942	216.60455	-2776.34839
HCHO	25.89749	105.63150	-70.78465	19.47195	-0.36586	-2108.63836	54.92340	-2095.58184
HCOOH	21.78722	158.24391	-109.11898	29.81645	-0.03715	-2850.83487	65.11810	-2838.08610
CH_3OH	11.94820	182.36680	-114.91865	30.33870	0.24340	-2831.65372	46.51922	-2821.75746
CO_2	40.08624	50.31535	-30.37540	7.04861	-0.24033	-2209.24245	109.49837	-2194.50276
H_2	43.03711	-4.78643	4.59162	-0.48639	-0.18453	-637.06482	113.92258	-623.78751
HCOO	19.74028	136.68582	-99.86426	27.90596	-0.03027	-2556.31361	50.53736	-2545.07842
COOH	32.71577	116.88908	-91.53825	27.44835	-0.39032	-2492.38257	72.42906	-2476.87835
CH_2OH	28.04684	132.28550	-88.69061	24.97058	-0.46393	-2442.62255	57.14691	-2427.55890
CH_3O	8.88349	158.86268	-99.26964	25.35178	0.23156	-2505.19028	29.56572	-2497.08434
H	-10.00132	79.34400	-69.38673	21.73208	-0.20534	-344.22718	-32.31878	-343.56384
CHO	27.08697	70.62429	-45.77631	11.73323	-0.17773	-1759.78192	65.42375	-1748.35204
CO	33.84550	19.75751	-8.02406	0.59040	-0.05167	-1517.15455	83.76401	-1506.08177
H_2O	42.83236	17.26276	-3.25359	0.74294	-0.33049	-1356.49011	106.14414	-1341.87117
OH	39.66391	1.95729	0.04527	0.76961	-0.71306	-1025.40651	69.32687	-1011.10017
HCOOHHCHO	21.33615	328.47776	-231.23890	63.19696	0.03972	-4981.53866	57.28476	-4962.62880
$HCOOCH_2OH$	39.33502	283.57288	-197.04706	54.54599	-0.36655	-5028.00150	82.17073	-5004.07354

CO_2CH_2OH	68.44144	181.58231	-118.23206	31.78177	-0.70223	-4662.23065	162.12512	-4632.38056
$CH_3OHHCOO$	24.07094	330.77713	-219.85782	58.64082	0.34087	-5405.47743	81.72256	-5386.56852
HCHOCOOH	42.26640	246.18960	-168.87179	45.38438	-0.20629	-4629.05681	101.79898	-4606.22311
CH_2OHCOO	46.15065	240.21448	-166.03162	45.11005	-0.44945	-4636.50712	98.76411	-4611.94078
CH_3OHCOO	33.57049	282.33868	-186.53184	49.12130	0.07488	-5029.74167	86.48581	-5008.98563
HCOOHbHCOO	26.56640	321.65183	-224.53645	60.49053	0.34994	-5430.25400	86.43749	-5411.07474
HCOOHmHCOO	28.88002	316.10944	-219.30521	58.75690	0.43319	-5379.68668	102.22086	-5360.30039
COOHOH	50.40151	159.10363	-113.58444	31.61561	-0.63049	-3539.47616	100.18044	-3516.20367

Elementary reactions	**A**	**B**	**C**	**D**	**E**	**F**	**G**	**H**
R1 HCOOH* + 2* ↔ HCOO* + H*	21.46931	171.24184	-130.27626	37.45864	-0.24144	-2814.25986	49.42339	-2800.51479
R3 HCOO* ↔ CO_2 + H*	29.90602	111.11450	-81.63178	22.39685	-0.18398	-2465.94417	79.32434	-2452.14887
R2 HCOOH* + * ↔ COOH* + H*	26.99344	160.77478	-125.76757	37.25448	-0.38701	-2758.00316	58.21793	-2742.54861
R4 COOH* + * ↔ CO_2* + H*	40.01573	102.41227	-81.27049	23.67749	-0.42566	-2402.45767	92.19181	-2385.21863
R9 H* + H* ↔ H_2* + *	11.25596	51.99429	-36.47410	9.62181	-0.25074	-610.15274	15.80133	-603.94804
R5 HCHO* + H* ↔ CH_2OH* + *	28.74866	134.74504	-94.36007	26.39306	-0.44308	-2370.69437	65.27723	-2355.42938
R6 HCHO* + H* ↔ CH_3O* + *	14.04898	160.80645	-112.45939	30.97081	-0.08640	-2420.41301	33.11258	-2408.71953
R7 CH_2OH* + H* ↔ CH_3OH* + *	18.52433	182.32750	-126.81635	35.72838	-0.29166	-2709.68023	42.82719	-2696.12487
R8 CH_3O* + H* ↔ CH_3OH* + *	12.52339	190.15301	-126.44285	33.71249	0.00595	-2737.87614	32.64913	-2726.76102
R10 HCHO* + * ↔ CHO* + H*	17.87592	124.63290	-90.60947	25.27413	-0.16378	-2050.49166	41.64348	-2039.82367
R11 CHO* + * ↔ CO* + H*	23.36159	58.05102	-31.70460	6.44998	0.03491	-1744.08053	67.09041	-1734.91954
R14 COOH* + * ↔ CO* + OH*	34.87174	96.93363	-76.65934	23.36966	-0.37285	-2434.81701	82.46524	-2419.49217
R13 H* + OH* ↔ H_2O* + *	38.49465	43.78294	-37.32699	12.68025	-0.93476	-1255.93395	66.06712	-1239.68026
R22(a) HCHO* + HCOOH* ↔ HCOOHHCHO*	39.80454	261.33521	-177.73822	48.68758	-0.41349	-4948.01168	93.01812	-4924.61567
R22(b) HCOOHHCHO* ↔ $HCOOCH_2OH$*	19.81347	324.22713	-233.70031	65.24348	-0.19275	-4977.54920	45.40904	-4958.52025
R22(c) $HCOOCH_2OH$* + * ↔ CO_2CH_2OH* + H*	70.04275	216.66559	-148.41464	41.03959	-0.91700	-4953.81629	155.90176	-4921.45743

R22(d) CO_2CH_2OH* ↔ CO_2(g) + CH_2OH* + *	58.10632	176.25564	-113.14609	30.09665	-0.62485	-4629.66947	332.18398	-4603.35547
R25(a) CH_3O* + HCOOH* ↔ $CH_3OHHCOO$*	24.41891	312.30629	-203.68561	53.54825	0.24345	-5344.94255	78.76188	-5326.29128
R25(b) $CH_3OHHCOO$* + * ↔ HCOO* + CH_3OH*	23.13163	319.25978	-214.44644	57.99356	0.30542	-5387.54403	74.45167	-5369.26163
R23(a) HCHOCOOH* ↔ CH_2OHCOO*	33.95699	246.17678	-168.85965	45.38034	-0.19230	-4628.48391	77.37239	-4608.17506
R23(b) CH_2OHCOO* ↔ CO_2(g) + CH_2OH* + *	49.33803	210.25375	-140.93828	37.88988	-0.51983	-4627.09281	109.71266	-4602.46435
R24(a) CH_3O* + COOH* ↔ CH_3OHCOO*	30.55602	278.07159	-189.14592	51.44164	-0.02883	-4998.76301	79.49052	-4978.76605
R24(b) CH_3OHCOO* ↔ CH_3OH* + CO_2(g) + *	37.34337	250.35731	-159.32230	41.12039	0.05111	-5017.51502	101.52266	-4996.75127
R26(a) HCOOH* + HCOO* ↔ HCOOHbHCOO*	34.77988	293.19579	-209.86669	58.60474	-0.06967	-5414.04809	94.09141	-5392.15149
R26(b) HCOOHbHCOO* ↔ HCOOHmHCOO* + *	23.85646	310.32191	-216.30222	58.39554	0.37838	-5370.66595	88.26841	-5352.82501
R24(c) HCOOHmHCOO* + HCOO* ↔ HCOOHbHCOO* + CO_2(g) + H*	56.16210	434.75915	-309.10579	84.10449	0.12137	-7921.89143	158.25949	-7888.79481
R14(a) COOH* + OH* ↔ COOHOH*	66.29945	113.42977	-86.22724	26.45229	-0.94142	-3517.32699	131.42851	-3490.07022
R14(b) COOHOH* ↔ CO_2* + H_2O*	70.01800	85.23705	-49.82013	12.63748	-0.62376	-3523.86379	167.40526	-3497.52250

Table S5 Shomate parameters for the transition states of all elementary steps on clean Cu(111).

S5 NEB structures for all elementary steps on clean Cu(111)

Figure S2 shows DFT structure of the initial state (IS), transition state (TS) and final state (FS) of each elementary step for NEB calculation on clean Cu(111) surface. All elementary steps here correspond to the steps shown in Table S5. For each elementary step, we explore several possible pathways from the initial state to the final state, and we choose the pathway with the lowest transition state energy, sequentially, the Shomate parameters of this lowest-energy transition state are calculated using methods described in S3. Some elementary steps go through two transition states, in this case, the transition state with the highest energy is counted for Shomate parameters calculation (for example, HCOO* ↔□ CO_2* + H* has TS1 and TS2, TS2 has higher energy than TS1, therefore, TS2 is considered the transition state for this elementary step). For some direct hydrogen transfer elementary steps, their NEB structures are combined together to better illustrate the reaction flow.

R1 HCOOH* + 2* ↔□ HCOO* + H*

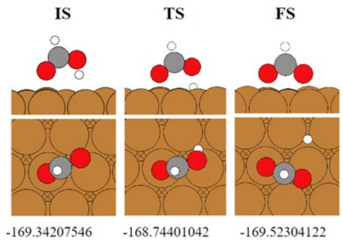

R3 HCOO* ↔□ CO_2 + H*

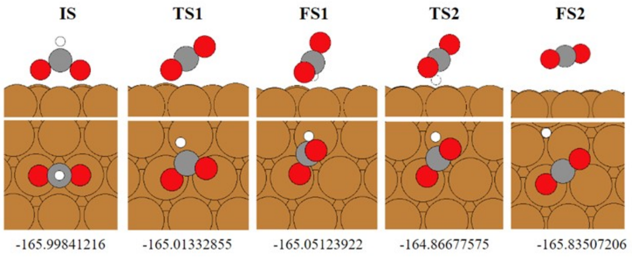

R2 HCOOH* + * ↔□ COOH* + H*

R4 COOH* + * ↔□ CO_2* + H*

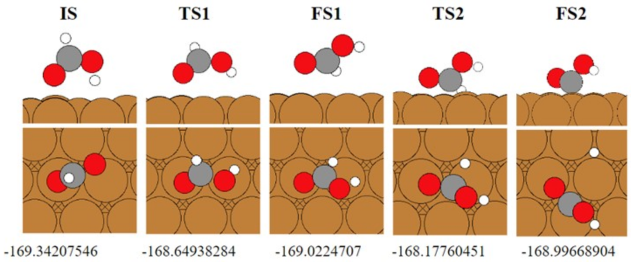

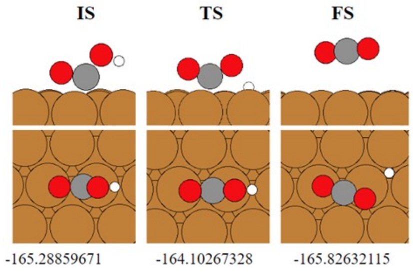

R9 $H^* + H^* \leftrightarrow H_2^* + *$

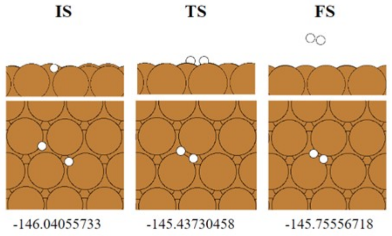

R5 $HCHO^* + H^* \leftrightarrow CH_2OH^* + *$

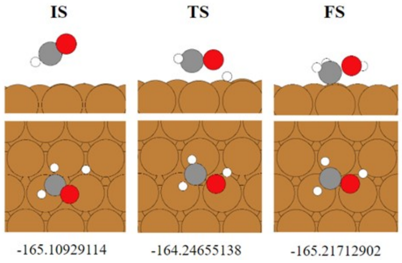

R6 $HCHO^* + H^* \leftrightarrow CH_3O^* + *$

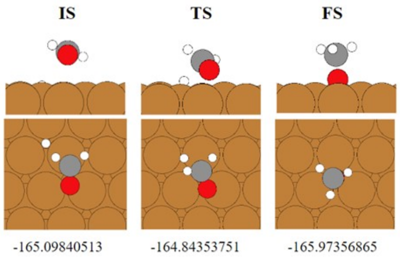

R7 $CH_2OH^* + H^* \leftrightarrow CH_3OH^* + *$

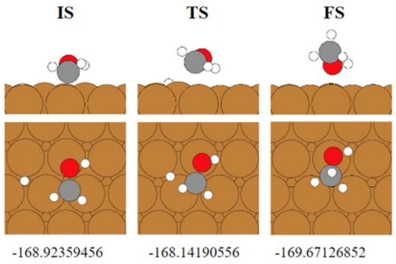

R8 $CH_3O^* + H^* \leftrightarrow CH_3OH^* + *$

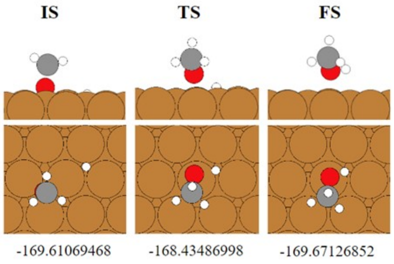

R10 $HCHO^* + * \leftrightarrow CHO^* + H^*$

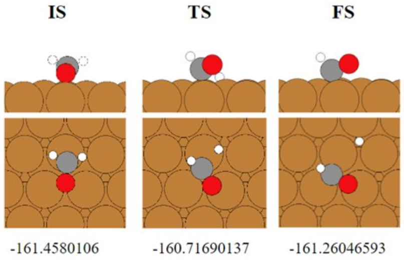

R11 $CHO^* + {}^* \leftrightarrow$□ $CO^* + H^*$

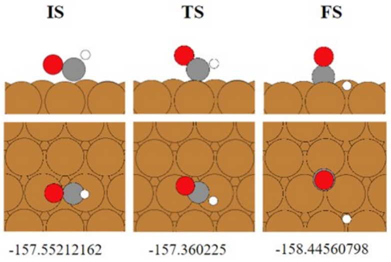

R12 $COOH^* + {}^* \leftrightarrow$□ $CO^* + OH^*$

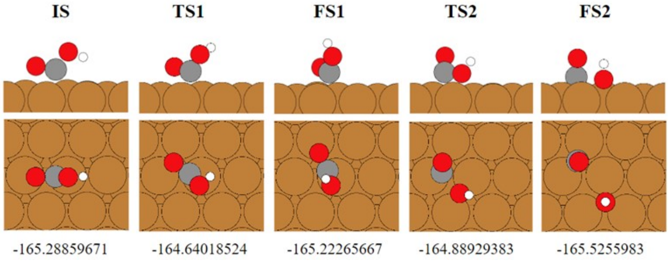

R13 $H^* + OH^* \leftrightarrow$□ $H_2O^* + {}^*$

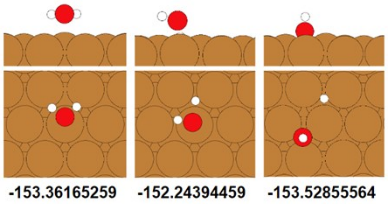

R22(a) $HCHO^* + HCOOH^* \leftrightarrow$□ $HCOOHHCHO^*$

R22(b) $HCOOHHCHO^* \leftrightarrow$□ $HCOOCH_2OH^*$

R22(c) $HCOOCH_2OH^* + {}^* \leftrightarrow$□ $CO_2CH_2OH^* + H^*$

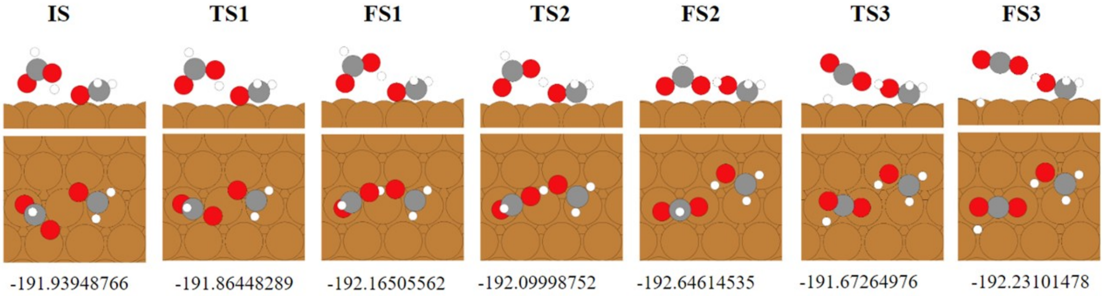

R22(d) $CO_2CH_2OH^* \leftrightarrow$□ $CO_2(g) + CH_2OH^* + {}^*$ [1]

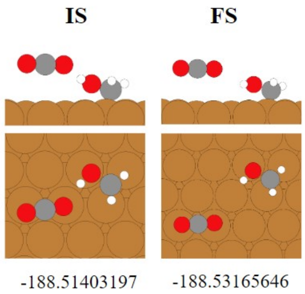

[1] NEB calculation is not applied for this step, because since a gas phase molecule is involved in this reaction, we assume the reverse step is inactivated similar to adsorption of CO_2(g), as no covalent bond is formed or broken. Therefore, for this step, we use the FS's structure for vibrational frequency calculation to get Shomate parameters, and used it as the transition state's Shomate parameters.

R25(a) $CH_3O^* + HCOOH^* \leftrightarrow CH_3OHHCOO^*$

R25(b) $CH_3OHHCOO^* + {}^* \leftrightarrow HCOO^* + CH_3OH^*$

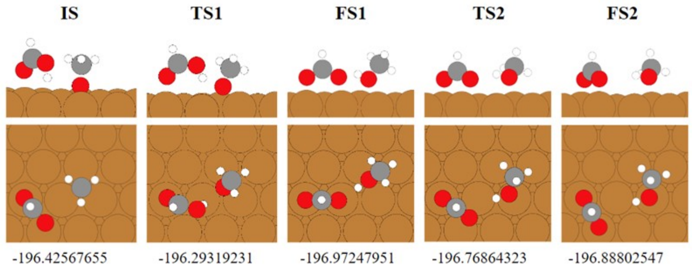

R23(a) $HCHOCOOH^* \leftrightarrow CH_2OHCOO^*$

R23(b) $CH_2OHCOO^* \leftrightarrow CO_2(g) + CH_2OH^* + {}^*$

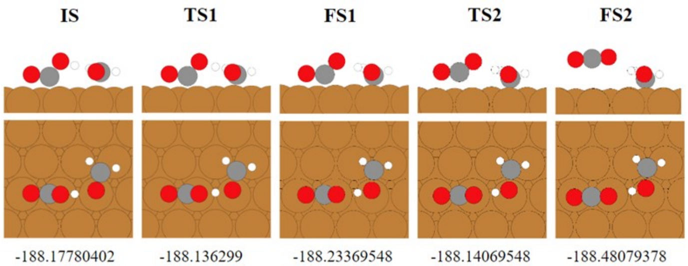

R24(a) $CH_3O^* + COOH^* \leftrightarrow$□ CH_3OHCOO^*

R24(b) $CH_3OHCOO^* \leftrightarrow$□ $CH_3OH^* + CO_2(g) + {}^*$

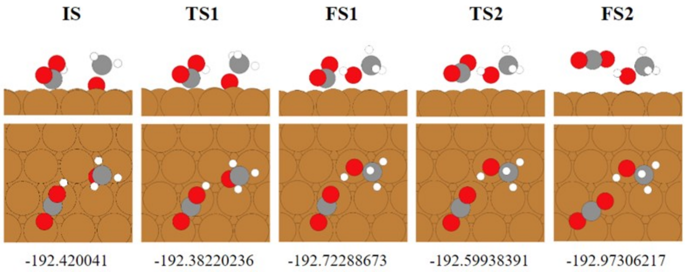

R26(a) $HCOOH^* + HCOO^* \leftrightarrow$□ $HCOOHbHCOO^*$

R26(b) $HCOOHbHCOO^* \leftrightarrow$□ $HCOOHmHCOO^* + {}^*$

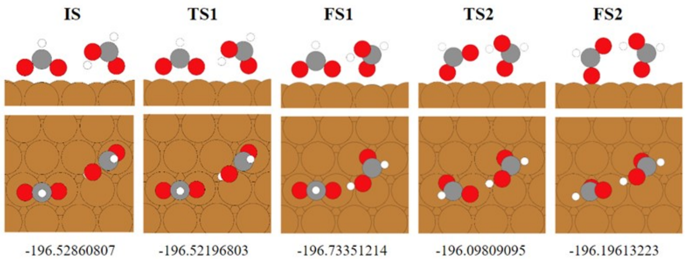

R26(c) $HCOOHmHCOO^* + HCOO^* \leftrightarrow$□ $HCOOHbHCOO^* + CO_2(g) + H^*$

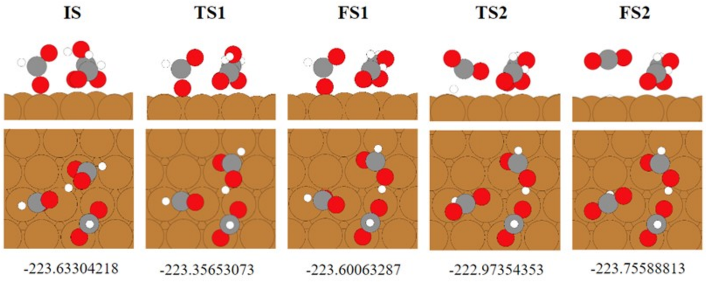

R14(a) $COOH^* + OH^* \leftrightarrow$□ $COOHOH^*$

R14(b) $COOHOH \leftrightarrow$□ $CO_2^* + H_2O^*$

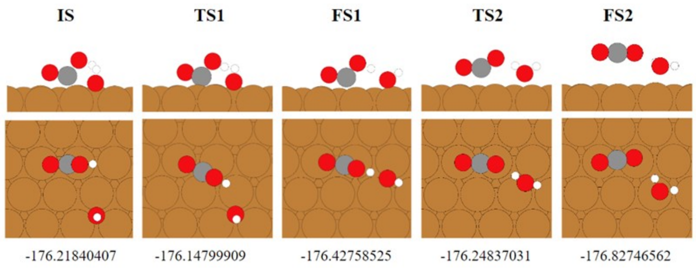

Figure S2 NEB structures for all elementary steps on clean Cu(111) applied in MKM. Copper atoms are in orange, carbon in grey, oxygen in red, and hydrogen in white. DFT energy for each structure is denoted below.

S6 Results of the first (no corrections) and second (approximate corrections) iterations and model predictions

In our first iteration, where we applied no surface corrections, both models showed that the surface was heavily covered; specifically, the "HCOOH-cofeed" model showed 2/9th monolayer (ML) of HCOO* (which is bidentate and hence covers ~ 44% of all sites) and 5/9th ML of H*; while "H_2-cofeed" model was entirely covered by CH_3O* (~1ML) at 373K, 1 atm, with partial pressure of HCHO and HCOOH/H2 being 0.15 and 0.08 respectively (and rest inert). High coverage of intermediates indicates the need to include coverage-dependent corrections to destabilize surface intermediates and transition states. Therefore, we included an approximate destabilization model with respect to HCOO* and CH_3O*. Since our DFT calculations showed that the relative energy of HCOO* (-0.61 eV) changes by less than 0.1 eV when H* coverage was changed from 0 to 4/9th ML (as shown in Table S6), in addition, our subsequent MKM models didn't demonstrate high H* coverage, hence we did not add any destabilization corrections for H*.

Specifically, relative energies of HCOO* on different H* coverage Cu(111) surface are calculated using H*-covered surface as reference, for example, the relative energy of HCOO* on 2/9th ML H*-covered surface are calculated as:

$$RE\left(HCOO^{*}\ on\ \frac{2}{9}ML\ H^{*}\ covered\ surface\right) = E\left(HCOO^{*} + 2H^{*}\right) - E\left(2H^{*}\right) - E\left(HCOOH(g)\right) + \frac{1}{2}E\left(H_2(g)\right)$$

Table S6 Relative energies of HCOO* in presence of different H* coverage on Cu(111)

Surface coverage of H* / ML	RE(HCOO*) on H*-covered surface / eV
0	-0.61
1/9th	-0.58
2/9th	-0.52
3/9th	-0.55
4/9th	-0.51
5/9th	-0.31

For the second iteration, the DFT-derived differential binding energies of HCOO* and CH_3O* were computed for varying surface coverage values (up to 4/9th ML) of the respective species; polynomial models were fitted to these data and employed as self-destabilization terms f(θ) in the microkinetic model. Additionally, cross-destabilization was included, i.e., the destabilization of other species by HCOO* and CH_3O* by using the same self-destabilization models f(θ) as a first approximation. Furthermore, the transition state energies (and, hence, the activation barriers) were also corrected for HCOO* and CH_3O* coverages using self-destabilization model parameters accounting for the number of reactants. The destabilization corrections f(θ) applied to enthalpy were applied as a complement to the enthalpy derived from Shomate parameters. The destabilization parameters are shown in Table S7.

Table S7 Polynomial expression ($f(\theta) = \alpha_0 + \alpha_1\theta + \alpha_2\theta^2 + \alpha_3\theta^3$) for destabilizing the enthalpy of the adsorbates and transition states by surface coverage of CH_3O^* and $HCOO_X^*$ ($HCOO_X^*$ = $HCOO^*$ + $HCOOCH_2OH^*$ + HCOOHbHCOO*). Polynomial coefficients are calculated by fitting the binding energy (in kJ/mol) of CH_3O^*/$HCOO^*$ under different coverage of $\theta(CH_3O^*)/\theta(HCOO^*)$ on Cu(111) (e.g. binding energy of CH_3O^* on 1/9ML CH_3O^*, 2/9ML CH_3O^* and 3/9ML CH_3O^* covered Cu(111) surface). α_0 are forced to be zero and α_1 are forced to be non-negative for ensuring destabilization.

Destabilization reference species	α_0	α_1	α_2	α_3
CH_3O^*	0	0	1111.55835	-2388.80877
$HCOO_X^*$	0	74.59692	-1671.52700	8889.55375

Although the cross-destabilization approximation, in lieu of deriving detailed models from DFT calculations for each species, simplifies the treatment of energetics, the microkinetic models still provide valuable chemical insights and guides next steps. First, formic acid leads to a higher hydrogenation rate than the traditional molecular H_2. Figure 6 (a) compares the hydrogenation rate for our "HCOOH-cofeed" and "H_2-cofeed" versions under various temperature conditions while total pressure is 1 atm with partial pressure of HCHO and HCOOH (or H_2) being 0.15 and 0.08 respectively (and rest inert) .The methanol formation rate (the turnover frequency) is eight orders of magnitude higher for the HCOOH-cofeed case compared to the H_2-cofeed case when the effective amount of H atoms fed is the same in both cases.

Second, hydrogen bonding plays an important role in transfer hydrogenation of HCHO. Figure 6 (b) shows the reaction fluxes through the network and the predicted surface coverages under a representative condition of at 373K, 1 atm, with partial pressure of HCHO and HCOOH (or H_2) being 0.15 and 0.08 respectively (and rest inert) for "HCOOH-cofeed" model. In the most dominant pathway of HCHO hydrogenation on clean Cu(111) surface, HCHO* preferred to pick up a surface H* and form an adsorbed methoxy ($HCHO^* + H^* \leftrightarrow$ $CH_3O^* + *$), then the carbonyl oxygen of CH_3O^* could form a hydrogen bond with the hydroxy group of HCOOH resulting in the formation of CH_3OH^* ($HCOOH^* + CH_3O^* \leftrightarrow$ $CH_3OHHCOO^* \leftrightarrow$ $HCOO^* + CH_3OH^*$). Therefore, the first hydrogenation of HCHO* to CH_3O^* is via the indirect hydrogen transfer route (i.e. with an addition of a surface H* to HCHO* to form CH_3O^*), but the second hydrogenation step from CH_3O^* to CH_3OH^* was favored via direct hydrogen transfer facilitated by hydrogen bonding. The flux of this hydrogenation pathway involving a direct hydrogen atom transfer step is at least 9 orders of magnitude larger than a purely indirect pathway (i.e. successive hydrogenation by a H* in the "H2-cofeed" model), thereby explaining the higher activity in the case of HCOOH cofeed.

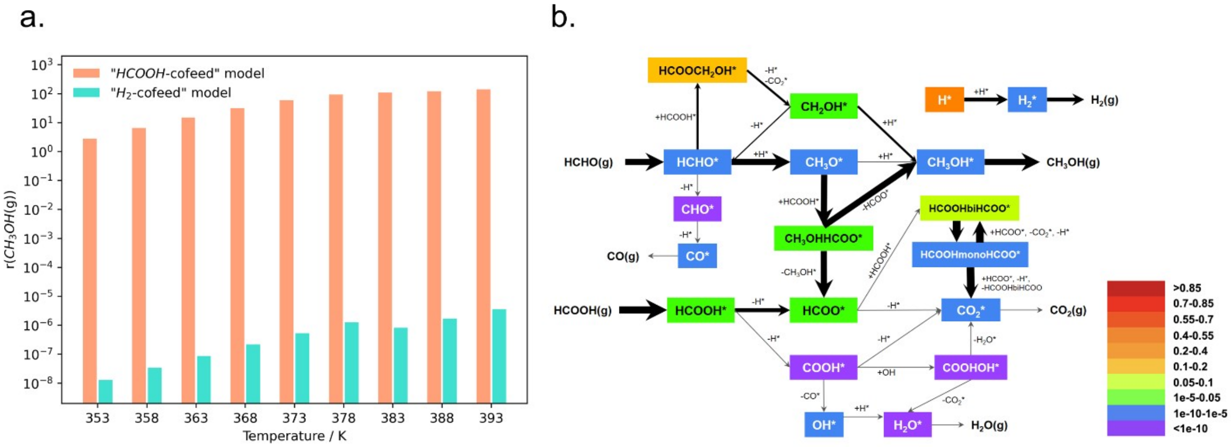

Figure S3: MKM results of the second iteration. (a) Comparison of the hydrogenation rate of "HCOOH-cofeed" model and "H_2-cofeed" model under various temperature, total pressure of 1 atm, with partial pressure of HCHO and HCOOH/H_2 being 0.15 and 0.08 respectively (and rest inert). (b) Reaction network for "HCOOH-cofeed" model at 373K, 1 atm, with partial pressure of HCHO and HCOOH being 0.15 and 0.08 respectively (and rest inert). The width of the arrows qualitatively represented the magnitude of the reaction flux, and the coverages of surface intermediate were color coded by different level.

In an alternative pathway for HCHO hydrogenation, that has a flux almost sixty (60) times lower than the most dominant one, the first hydrogenation step from HCHO* to CH_2OH* occurred via hydrogen transfer from HCOOH* to HCHO* via a hydrogen-bonded intermediate and the second hydrogenation step from CH_2OH* to CH_3OH* preferred surface hydrogenation with H*. The H-bond mediated reaction proposed by Chen and Mavrikakis[2,3], viz. HCOOH co-catalyzed HCOO decomposition, had the highest rate in our model. The high coverage of H* could also be attributed to the substantial flux associated with this reaction. At the chosen reaction condition, the surface is still heavily covered by intermediates, the most abundant surface intermediate is H* (~5/9th ML), and the coverage of all HCOO*-related species is around 2/9th ML. On the other hand, the "H_2-cofeed" model exhibits a 3/9th ML CH_3O* coverage and 6/9th ML vacant sites.

Our model averagely predicted surface coverage of 2/9th ML $HCOO_X$* ($HCOO_X$* is a congregation of HCOO* and all HCOO*-related hydrogen-bonded complex), 5/9th ML H* and 0.01 ML vacant sites for "HCOOH-cofeed" model. Our "H_2-cofeed" model demonstrated a higher 5/9th ML CH_3O* coverage and 4/9th ML CO* coverage at lower temperature (353K-378K), and a 3/9th ML CH_3O* coverage and 6/9th ML vacant sites at higher temperature (383K - 423K), the discrepancy of CH_3O* coverage under different temperature was probably caused by HCHO decomposition at lower temperature. Comparing to the model results from the first iteration, we observe a significant coverage change for the "H_2-cofeed" case, whereas there is no notable change for the "HCOOH-cofeed" case. The model results from the second iteration lack the requisite robustness to definitively conclude the intermediates' coverage. However, it demonstrates that the "HCOOH-cofeed" model gave a substantially higher rate than "H_2-cofeed" case.

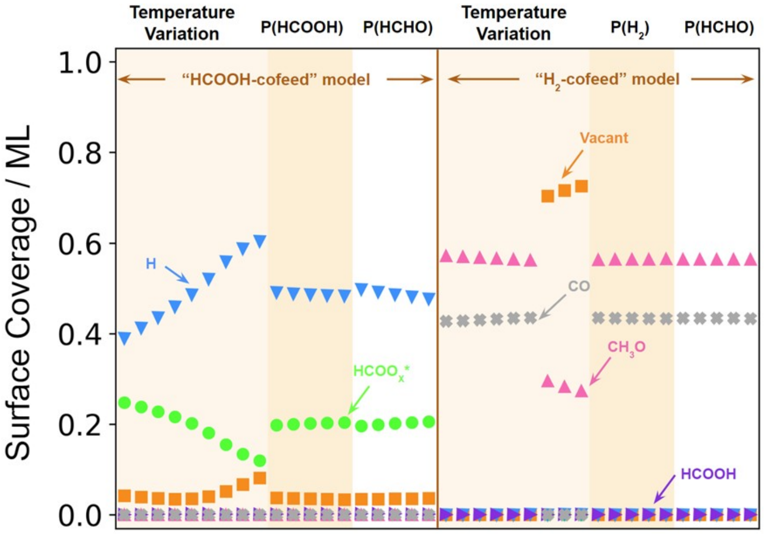

Figure S4 Coverages of relevant reaction intermediates under various reaction conditions as predicted by the second iteration of "HCOOH-cofeed" mode (left half) and "H_2-cofeed" model (right half). For each half, shaded areas from left to right represent different reaction conditions: temperature variation from 353K to 393 K with increments of 5K (points #1-#9 and #20-#28), partial pressure of HCOOH or H2 variation from 0.062 to 0.092 with increments of 0.0077 (#10-#14 and #29-#33), partial pressure of HCHO variation from 0.14 to 0.17 with increments of 0.0077 (#15-#19 and #34-#38).

S7 DFT structure of the most stable adsorption states of intermediates on 3/9th MLCH$_3$O*-covered surface

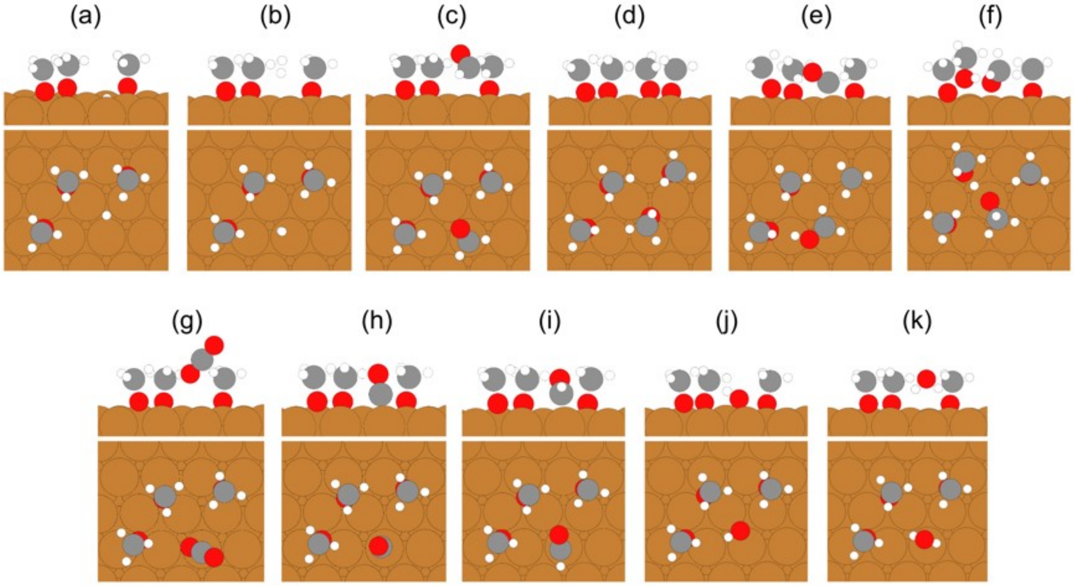

Figure S5: Most stable adsorption states of selected intermediates on 3/9th ML CH_3O^*-covered Cu(111) surface. 3/9th ML CH_3O^* translates to 3 CH_3O^* per 9 Cu atoms. For each row, the top part is the front view, and the bottom part is the top view. First row: (a) atomic hydrogen, (b) molecular hydrogen, (c) formaldehyde, (d) methoxy, (e) hydroxymethyl, (f) methanol. Second row: (g) carbon dioxide, (h) carbon monoxide, (i) hydroxymethylidyne, (j) hydroxide, (k) water. Copper atoms are in orange, carbon in grey, oxygen in red, and hydrogen in white.

S8 NEB structures for selected elementary steps at 2/9th ML HCOO*-covered surface for "HCOOH-cofeed" model

Here, we demonstrate DFT structure of the initial state (IS), transition state (TS) and final state (FS) of each selected elementary step for NEB calculation on 2/9th ML HCOO*-covered Cu(111) surface. All elementary steps here correspond to the steps shown in Table S10. For each elementary step, we explore several possible pathways from the initial state to the final state, and we choose the pathway with the lowest transition state energy, sequentially, the Shomate parameters of this lowest-energy transition state are calculated using methods described in S3. Some elementary steps go through two transition states, in this case, the transition state with the highest energy is counted for Shomate parameters calculation (for example, $HCOO^*$ ↔□ CO_2^* + H^* has TS1 and TS2, TS1 has higher energy than TS2, therefore, TS1 is considered the transition state for this elementary step). For some direct hydrogen transfer elementary steps, their NEB structures are combined together to better illustrate the reaction flow.

Note that for elementary step $HCOOH^*$ + $HCOO^*$ ↔□ $HCOOH^*$ + $CO_2(g)$ + H^* + *, when we build NEB calculation for this step on clean Cu(111) surface, we consider the effect of hydrogen bonding change from one $HCOO^*$ to the other, so the surface already exists two $HCOO^*$ molecules (as shown in S4 HCOOHmHCOO* + $HCOO^*$ ↔□ HCOOHbHCOO* + $CO_2(g)$ + H^*), therefore, it's not necessary to recalculate the NEB for this elementary step on 2/9th ML $HCOO^*$-covered surface. However, the Shomate parameters calculation for this step is corrected, more details could be found in S10 notation.

R1 $HCOOH^* + 2^*$ ↔□ $HCOO^* + H^*$

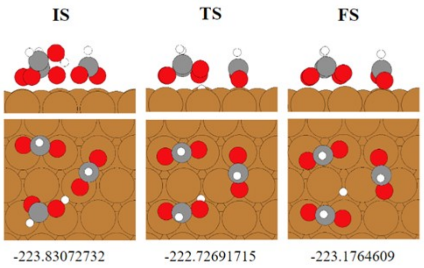

R3 $HCOO^*$ ↔□ $CO_2^* + H^*$

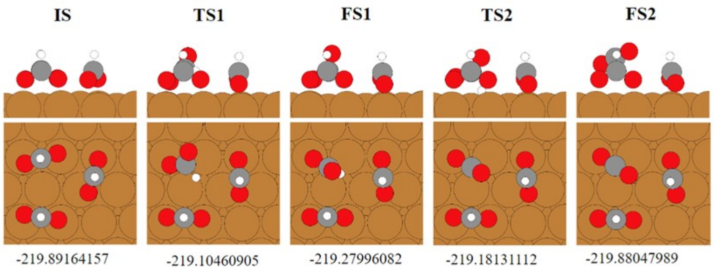

R9 H^* +H^* ↔□ H_2^* + *

R5 $HCHO^*$ + H^* ↔□ CH_2OH^* + *

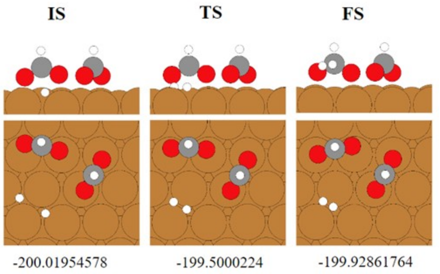

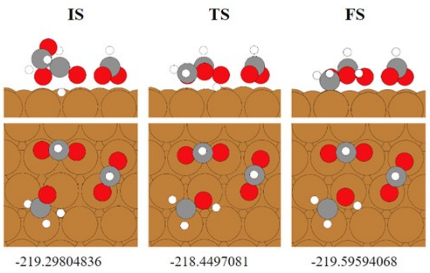

R6 HCHO* + H* ↔□ CH_3O* + *

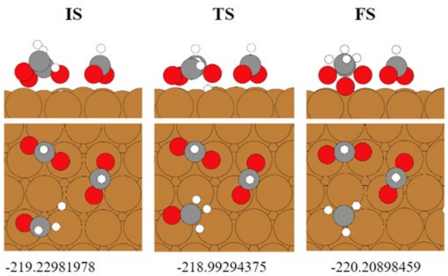

R7 CH_2OH* + H* ↔□ CH_3OH* + *

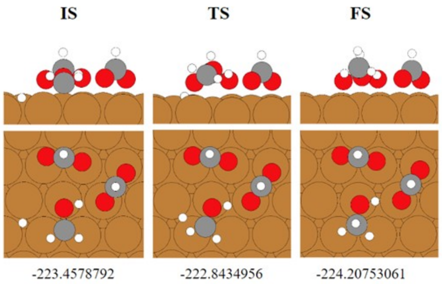

R8 CH_3O* + H* ↔□ CH_3OH* + *

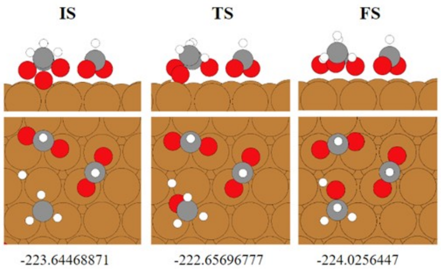

R25(a) CH_3O* + HCOOH* ↔□ $CH_3OHHCOO$*

R27 $CH_3OHHCOO$* ↔□ CH_3OH* + CO_2(g) + H*

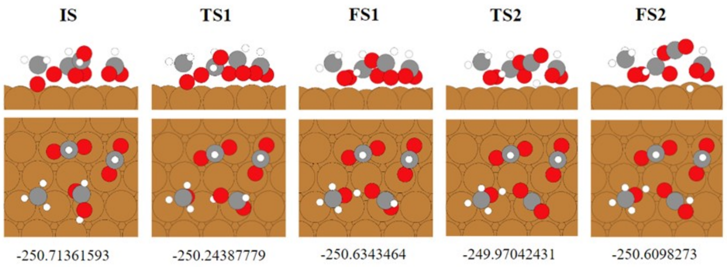

R25(b) $CH_3OHHCOO^*$ ↔□ $CH_3OH(g) + HCOO^*$ R22 $HCHO^* + HCOOH^* + {}^*$ ↔□ $CH_2OH^* + HCOO^*$

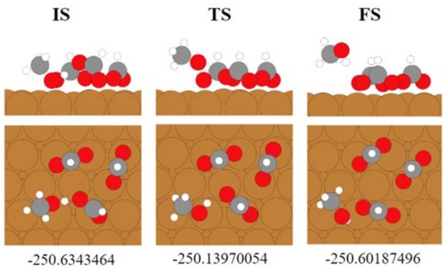

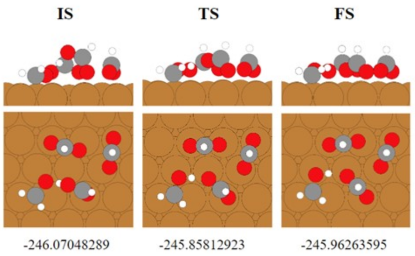

Figure S6 NEB structures for selected elementary steps at 2/9th ML $HCOO^*$-covered surface for “HCOOH-cofeed” model. Copper atoms are in orange, carbon in grey, oxygen in red, and hydrogen in white. DFT energy for each structure is denoted below.

S9 NEB structures for selected elementary steps at 3/9th ML CH_3O^*-covered surface for "H_2-cofeed" model

Here, we demonstrate DFT structure of the initial state (IS), transition state (TS) and final state (FS) of each selected elementary step for NEB calculation on 3/9th ML CH_3O^*-covered Cu(111) surface for "H_2-cofeed" model. the activation energy of each step is compared between 3/9th ML CH_3O^*-covered Cu(111) surface and clean Cu(111) surface, to obtain the linear expression (ΔE_{TS} (in kJ/mol) = $\alpha_0 + \alpha_1\theta$) for cross-destabilization (corresponding to table S17). For each elementary step, we explore several possible pathways from the initial state to the final state, the pathway with the lowest transition state energy is chosen.

R6 $HCHO^* + H^* \leftrightarrow$□ $CH_3O^* + *$

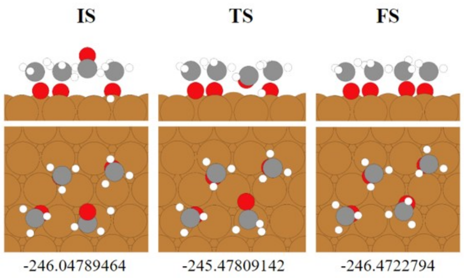

R8 $CH_3O^* + H^* \leftrightarrow$□ $CH_3OH^* + *$

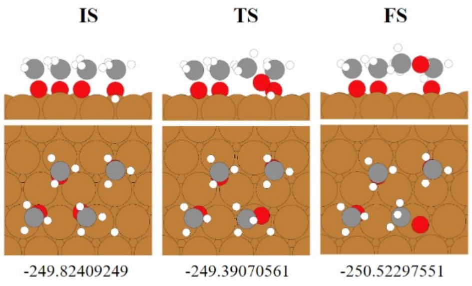

R9 $H^* + H^* \leftrightarrow$□ $H_2^* + *$

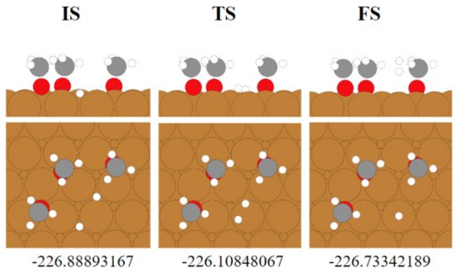

Figure S7 NEB structures for selected elementary steps at 3/9th ML CH_3O^*-covered surface for "H_2-cofeed" model. Copper atoms are in orange, carbon in grey, oxygen in red, and hydrogen in white. DFT energy for each structure is denoted below.

S10 binding energy of surface intermediates on clean surface, 2/9th ML HCOO*-covered surface and 3/9th MLCH_3O*-covered surface

Table S8 The binding energies of surface intermediates defined in 3.2.1 on clean Cu(111) surface, 2/9th ML HCOO*-covered Cu(111) surface and 3/9th ML CH_3O*-covered Cu(111) surface. Since the 3/9th ML CH_3O*-covered Cu(111) surface only appears in H_2-cofeed case, the binding(relative) energy of HCOOH, HCOO and COOH in the presence of 3/9th ML CH3O* are not calculated. This table is a supplement for Figure 9.

Surface intermediates	**BE, Clean surface /eV**	**BE, 2/9th ML HCOO*-covered surface /eV**	**BE, 3/9th ML CH_3O*-covered surface /eV**
H_2O*	-0.42	-0.92	-0.60
CH_3OH*	-0.56	-0.88	-0.79
HCOOH*	-0.57	-0.83	
H_2*	-0.11	-0.27	-0.23
CO_2*	-0.24	-0.40	-0.30
COOH*	0.10	0.06	
CH_2OH*	0.51	0.11	0.53
OH*	-0.05	-0.08	0.18
CH_3O*	-0.25	-0.26	0.11
CHO*	0.08	0.32	-0.04
HCHO*	-0.44	-0.41	-0.67
HCOO*	-0.61	-0.28	
H*	-0.36	-0.24	-0.23
CO*	-1.10	-0.94	-1.06

S11 Shomate parameters for selected adsorbates and elementary steps (identified in section 3.2.1) at the reference coverage (2/9th ML HCOO*) for "HCOOH-cofeed" model

Table S9 Shomate parameters for selected adsorbates at 2/9th ML HCOO*-covered surface for "HCOOH-cofeed" model

Species	**A**	**B**	**C**	**D**	**E**	**F**	**G**	**H**
CH_3OH(g)	-5.29983	181.15146	-112.57259	29.30009	0.53265	-2777.14479	185.52218	-2773.39651
CO_2(g)	26.73128	51.97803	-31.76245	7.48792	-0.16811	-2185.59744	231.67315	-2175.01922
H_2(g)	30.31599	-3.69451	3.12604	0.01987	-0.03736	-627.55982	168.03767	-618.53237
HCHO(g)	5.14178	94.58192	-47.20776	8.88903	0.55499	-2061.42315	201.97497	-2057.94721
HCOOH(g)	7.49790	154.21035	-108.96994	30.64834	0.03472	-2795.22942	216.60455	-2787.15839
HCHO	23.65645	107.28575	-70.10370	18.78367	-0.26432	-2105.00808	47.59852	-2092.88209
HCOOH	8.31052	180.92877	-121.30912	31.64008	0.33670	-2872.50861	35.23093	-2864.12765
CH_3OH	3.13270	195.83476	-121.30971	31.13225	0.30247	-2860.04942	14.73014	-2852.43588
CO_2	39.82884	50.12415	-30.08184	6.96750	-0.25587	-2224.34729	106.36153	-2209.63828
H_2	33.39404	16.16044	-12.45274	4.71294	-0.69661	-653.45504	53.99037	-640.54460
HCOO	19.27479	135.57791	-97.77254	27.02733	-0.08710	-2524.95581	39.68113	-2513.70129
CH_2OH	16.15872	151.47240	-98.93278	26.67845	-0.35534	-2477.61578	16.32927	-2465.69513
CH_3O	8.50324	158.03079	-97.89392	24.81564	0.17961	-2506.71895	22.33081	-2498.57798
H	-15.06328	89.02486	-76.71469	23.76238	-0.07339	-330.84638	-42.13706	-331.76527
$CH_3OHHCOO$	11.60247	351.44742	-229.38841	59.30460	0.33505	-5348.97883	23.01108	-5332.93202

Table S10 Shomate parameters for selected elementary steps' transition states at 2/9th ML HCOO*-covered surface for "HCOOH-cofeed" model

Elementary reactions	**A**	**B**	**C**	**D**	**E**	**F**	**G**	**H**
R1 HCOOH* + 2* ↔□ HCOO* + H*	16.80738	180.33945	-137.57799	39.62705	-0.15560	-2789.63092	34.47775	-2777.21959
R3 HCOO* ↔□ CO_2* + H*	16.57517	124.48844	-88.62498	24.25486	0.00216	-2452.04675	46.21962	-2442.31404
R9 H* + H* ↔□ H_2* + *	-0.07868	82.61828	-65.29489	18.94552	-0.18517	-592.89353	-14.14004	-589.16324
R5 HCHO* + H* ↔□ CH_2OH* + *	21.03778	148.87034	-104.57448	29.10920	-0.39168	-2365.65757	38.29099	-2352.32102
R6 HCHO* + H* ↔□ CH_3O* + *	5.28629	178.19256	-126.22990	34.97163	0.03724	-2408.59858	11.05035	-2400.27338
R7 CH_2OH* + H* ↔□ CH_3OH* + *	0.11958	213.21052	-144.64938	39.05719	0.14417	-2748.53771	2.72920	-2740.70987
R8 CH_3O* + H* ↔□ CH_3OH* + *	5.11039	204.49798	-139.02328	37.79368	0.13931	-2733.23595	20.12445	-2724.24382
R25(a) CH_3O* + HCOOH* ↔□ $CH_3OHHCOO$*	21.85917	315.99139	-208.77267	55.77650	-0.04509	-5314.29312	38.19364	-5295.31402
R25(b) $CH_3OHHCOO$* ↔□ CH_3OH(g) + HCOO*	15.88714	330.57172	-221.78447	59.82081	0.11262	-5301.66471	33.07143	-5284.45403
R27 $CH_3OHHCOO$* ↔□ CH_3OH* + CO_2(g) + H*	35.83724	301.38157	-200.55880	53.50792	-0.25174	-5305.29105	74.02563	-5282.03254
R22 HCHO* + HCOOH* + * ↔□ CH_2OH* + HCOO*	15.83284	307.02530	-207.56871	55.33174	-0.45260	-4925.14193	-4.09243	-4906.98154
R26 HCOOH* + HCOO* ↔□ HCOOH* + CO_2(g) + H* + * [1]	36.38184	268.19862	-194.53241	54.70357	-0.34680	-5274.58772	275.81332	-5252.26730

[1] Shomate parameters of the transition state of the co-catalysis step, HCOOH* + HCOO* ↔□ HCOOH* + CO_2(g) + H* + *, is not calculated through NEB, but by correction of previously Shomate parameters of the same elementary step on clean Cu(111) surface.

Because for the same elementary step on clean Cu(111) surface, two HCOO* molecules already exist (as shown in S4 HCOOHmHCOO* + HCOO* ↔□ HCOOHbHCOO* + CO2(g) + H*). Therefore, the Shomate parameters are corrected in a way that consider the H-bonding effect on 2/9th ML HCOO*. Specifically, we calculate the difference of Shomate parameters between [the summation of HCOOH(g) and HCOO* on 2/9th ML HCOO*-covered surface] and [HCOOH* on 2/9th ML HCOO*-covered surface], then applies this difference to the previous Shomate parameters of the co-catalysis step on clean Cu(111) surface.

S12 Polynomial (or linear) parameters employed in the self-destabilization and cross-destabilization at the reference coverage (2/9th ML HCOO*) for "HCOOH-cofeed" model

Table S11 Linear expression ($f(\theta) = \alpha_0 + \alpha_1\theta$) for cross-destabilizing the binding energies of the selected adsorbates by 2/9th ML $HCOO_X$* ($HCOO_X$* = HCOO* + $CH_3OHHCOO$*) for "HCOOH-cofeed" model. Linear coefficients are calculated by using adsorbates' binding energy on 2/9th ML HCOO* as reference, and fitting the linear relationship with their binding energies on clean Cu(111) surface.

Destabilized adsorbates by $HCOO_X$*	α_0	α_1
HCOOH	25.86368	-116.38655
HCOO	-31.58520	142.13338
H	-11.63894	52.37523
CO_2	14.93119	-67.19034
HCHO	-2.79531	12.57891
CH_2OH	38.53663	-173.41484
CH_3O	1.43044	-6.43698
CH_3OH	30.45766	-137.05947
H_2	15.57472	-70.08626
$CH_3OHHCOO$	-63.85450	287.34525

Table S12 Linear expression ($f(\theta) = \alpha_0 + \alpha_1\theta$) for cross-destabilizing the transition states of the selected elementary steps by 2/9th ML $HCOO_X$* ($HCOO_X$* = HCOO* + $CH_3OHHCOO$*) for "HCOOH-cofeed" model. Linear coefficients for each step are calculated by using activation energies on 2/9th ML HCOO* and fitting the linear relationship with their activation energies on clean Cu(111) surface, and using 2/9th ML HCOO* as reference, then the coefficients of activation energies will be added with the corresponding coefficients of reactants, to obtain the destabilization coefficients for transition states (recall $E_{TS} = Ea + E_{IS}$).

Destabilized transition states by $HCOO_X$*	**α_0**	**α_1**
R1 HCOOH* + 2* ↔□ HCOO* + H*	73.55202	-330.98408
R3 HCOO* ↔□ CO_2* + H*	1.66402	-7.48808
R9 H* + H* ↔□ H_2* + *	-15.23128	68.54077
R5 HCHO* + H* ↔□ CH_2OH* + *	-4.84168	21.78756
R6 HCHO* + H* ↔□ CH_3O* + *	-6.86737	30.90317
R7 CH_2OH* + H* ↔□ CH_3OH* + *	46.41009	-208.84541
R8 CH_3O* + H* ↔□ CH_3OH* + *	-5.02352	22.60585
R25(a) CH_3O* + HCOOH* ↔□ $CH_3OHHCOO$*	-39.20442	176.41987
R25(b) $CH_3OHHCOO$* ↔□ CH_3OH(g) + HCOO*	-39.20442	176.41987
R27 $CH_3OHHCOO$* ↔□ CH_3OH* + CO_2(g) + H*	-39.20442	176.41987
R22 HCHO* + HCOOH* + * ↔□ CH_2OH* + HCOO*	-26.40223	118.81004

Table S13 Linear expression ($f(\theta) = \alpha_0 + \alpha_1\theta$) for cross-destabilizing the binding energy of the selected adsorbates by 3/9th ML CH_3O* for “HCOOH-cofeed” model. Linear coefficients are calculated by fitting the linear relationship between binding energy of each adsorbate on clean Cu(111) surface with 3/9th ML CH_3O* covered surface.

Destabilized adsorbates by CH_3O*	**α_0**	**α_1**

H	0	37.01353
CO_2	0	-16.49775
HCHO	0	-68.61809
CH_2OH	0	7.40384
CH_3OH	0	-65.37041
H_2	0	-33.74562

Table S14 Linear expression ($f(\theta) = \alpha_0 + \alpha_1\theta$) for cross-destabilizing the transition states of the selected elementary steps by 3/9th ML CH_3O^* for "HCOOH-cofeed" model. Linear coefficients are calculated by using activation energies of each step on 3/9th ML CH_3O^* and fitting the linear relationship with its activation energies on clean Cu(111) surface, then the coefficients of activation energies will be added with the corresponding coefficients of reactants, to obtain the destabilization coefficients for transition states (recall $E_{TS} = Ea + E_{IS}$).

Destabilized transition states by CH_3O^*	**α_0**	**α_1**
R9 $H^* + H^* \leftrightarrow H_2^* + {}^*$	0	54.01637
R6 $HCHO^* + H^* \leftrightarrow CH_3O^* + {}^*$	0	64.61763
R8 $CH_3O^* + H^* \leftrightarrow CH_3OH^* + {}^*$	0	-12.86982

Table S15 Polynomial expression ($f(\theta) = \alpha_0 + \alpha_1\theta + \alpha_2\theta^2 + \alpha_3\theta^3$) for self-destabilizing the binding energies of CH_3O^*, $HCOOH^*$, CH_3OH^*, $HCOO^*$ for "HCOOH-cofeed" model. Polynomial parameters for CH_3O^* are the same as Table S7. Polynomial parameters for $HCOO^*$ are corrected by using binding energy on 2/9th ML $HCOO^*$ as reference. For $HCOOH^*$ and CH_3O^*, binding energy of $HCOOH^*(CH_3O^*)$ on a surface with 2/9th ML $HCOO^*$ plus 1/9th ML

$HCOOH^*(CH_3O^*)$ are calculated, linear coefficients are then fitted by using binding energy of $HCOOH^*(CH_3O^*)$ on 2/9th ML $HCOO^*$ as reference.

Self-destabilizing species	α_0	α_1	α_2	α_3
CH_3O	0	0	1111.53640	-2388.76170
HCOOH	0	228.76795	0	0
CH_3OH	0	264.52404	0	0
HCOO	0	648.66696	4254.84217	8889.55376

S13 Linear parameters employed in the self-destabilization and cross-destabilization at the reference coverage (3/9th ML CH_3O^*) for "H_2-cofeed" model

Table S16 Linear expression ($f(\theta) = \alpha_0 + \alpha_1\theta$) for self- and cross- destabilizing the binding energy of the selected adsorbates by 3/9th ML CH_3O^* for "H_2-cofeed" model. Linear coefficients are calculated by fitting the linear relationship between binding energy of each adsorbate on clean Cu(111) surface and 3/9th ML CH_3O^* covered surface.

Destabilized adsorbates by CH_3O^*	α_0	α_1
H	0	37.01353
CO_2	0	-16.49775
HCHO	0	-68.61809
CH_2OH	0	7.40384
CH_3O	0	103.94081
CH_3OH	0	-65.37041
CHO	0	-37.06745
CO	0	16.66911

OH	0	68.23914
H_2O	0	-52.47452
H_2	0	-33.74562

Table S17 Linear expression ($f(\theta) = \alpha_0 + \alpha_1\theta$) for cross-destabilizing the transition states of the selected elementary steps by 3/9th ML CH_3O* for "H_2-cofeed" model. Linear coefficients are calculated by using activation energies of each step on 3/9th ML CH_3O* and fitting the linear relationship with its activation energies on clean Cu(111) surface, then the coefficients of activation energies will be added with the corresponding coefficients of reactants, to obtain the destabilization coefficients for transition states (recall $E_{TS} = Ea + E_{IS}$). This is identical to Table S14.

Destabilized transition states by CH_3O*	**α_0**	**α_1**
R9 H* + H* ↔□ H_2* + *	0	54.01637
R6 HCHO* + H* ↔□ CH_3O* + *	0	64.61763
R8 CH_3O* + H* ↔□ CH_3OH* + *	0	-12.86982

Reference

(1) Chase, M. W. Jr. NIST-JANAF Themochemical Tables, Fourth Edition. *J. Phys. Chem. Ref. Data* **1998**, *Monograph*.

(2) Chen, B. W. J.; Mavrikakis, M. Formic Acid: A Hydrogen-Bonding Cocatalyst for Formate Decomposition. *ACS Catal* **2020**, *10* (19). https://doi.org/10.1021/acscatal.0c02902.

(3) Chen, B. W. J.; Bhandari, S.; Mavrikakis, M. Role of Hydrogen-Bonded Bimolecular Formic Acid-Formate Complexes for Formic Acid Decomposition on Copper: A Combined First-Principles and Microkinetic Modeling Study. *ACS Catal* **2021**, *11* (7). https://doi.org/10.1021/acscatal.0c05695.